ORIGINAL ARTICLE

On-Machine Measurement of the Straightness and Tilt Errors of a Linear Slideway Using a New Four-Sensor Method

Lei Zhao[1], Kai Cheng[1,2], Hui Ding[1*] and Liang Zhao[1]

Abstract

Although there are some multi-sensor methods for measuring the straightness and tilt errors of a linear slideway, they need to be further improved in some aspects, such as suppressing measurement noise and reducing precondition. In this paper, a new four-sensor method with an improved measurement system is proposed to on-machine separate the straightness and tilt errors of a linear slideway from the sensor outputs, considering the influences of the reference surface profile and the zero-adjustment values. The improved system is achieved by adjusting a single sensor to different positions. Based on the system, a system of linear equations is built by fusing the sensor outputs to cancel out the effects of the straightness and tilt errors. Three constraints are then derived and supplemented into the linear system to make the coefficient matrix full rank. To restrain the sensitivity of the solution of the linear system to the measurement noise in the sensor outputs, the Tikhonov regularization method is utilized. After the surface profile is obtained from the solution, the straightness and tilt errors are identified from the sensor outputs. To analyze the effects of the measurement noise and the positioning errors of the sensor and the linear slideway, a series of computer simulations are carried out. An experiment is conducted for validation, showing good consistency. The new four-sensor method with the improved measurement system provides a new way to measure the straightness and tilt errors of a linear slideway, which can guarantee favorable propagations of the residuals induced by the noise and the positioning errors.

Keywords: Multi-sensor method, Straightness error, Tilt error, On-machine measurement, Linear slideway, Error separation technique

1 Introduction

Precision/ultra-precision products play an increasingly important role in many fields, such as daily life, national defense, military and aerospace, accordingly, the requirement for product accuracy in these fields is also becoming more stringent [1, 2]. For a machine tool/CMM, its accuracy is the crucial indicator which determines directly the accuracy and quality of machined products [3–5]. Therefore, it has been a major concern in the industry of how to improve the accuracy of a machine tool/CMM. As the essential element of a machine tool,

the linear slideway suffers from various errors, such as kinematic errors and errors induced by force. These errors change the geometric structure of the slideway, resulting in six geometric errors [6, 7]. These geometric errors include one positioning error, two straightness errors, two tilt errors and one roll error. The straightness and tilt errors not only reflect dynamically the operating status of a machine tool, but also are the key parameters of the error compensation model [8, 9]. Hence, it is of engineering and scientific significance for on-machine measuring the straightness and tilt errors of a linear slideway, especially for the case that the linear slideway works under the complicated condition.

The multi-sensor method is utilized widely to on-machine separate the surface profile from the sensor outputs [10]. The outputs are constructed by four

---

*Correspondence: dh_albert@126.com; dhalbert@hit.edu.cn
[1] School of Mechatronics Engineering, Harbin Institute of Technology, Harbin 150001, China
Full list of author information is available at the end of the article

Zhao *et al. Chin. J. Mech. Eng.*   (2019) 32:24

Page 2 of 11

parameters, namely the surface profile, the straightness and tilt errors of the linear slideway, as well as the zero-adjustment values of the sensors. After the surface profile is obtained, the straightness and tilt errors can be further identified. The two-sensor methods, such as the sequential two-sensor method [10, 11], the generalized two-sensor method [10, 11] and the combined two-sensor method [12], are used to estimate the surface profile without the tilt error and the zero-adjustment values. For the two-sensor methods, the harmonic suppression in the frequency domain results in that the reconstructed surface profile loses the harmonic components with the spatial period of an integer multiple of the sampling interval [11]. The sequential three-sensor method [10, 11], the generalized three-sensor method [11, 13] and the combined three-sensor method [14] are able to identify the surface profile, and the straightness and tilt errors. However, the zero-adjustment values will lead to large reduction in the accuracy of the reconstructed surface profile, even though they are tiny [11]. If the tilt error is measured in advance or ignored, the surface profile and the straightness error could be identified by using the three-sensor methods proposed by Yin, et al. [15, 16] and Fujimoto, et al. [17] respectively, considering the zero-adjustment values. The four-sensor method presented by Weingartner et al. [18] can reconstruct the surface profile in the presence of the straightness and tilt errors. However, it is affected significantly by the zero-adjustment values, and may not obtain the unique solution in some cases, due to the rank deficiency of the design matrix. Assuming that the tilt error is known in advance, Weingartner et al. [19] proposed another four-sensor method to evaluate the straightness and tilt errors as well as the zero-adjustment values. The solutions of the two four-sensor methods are very sensitive to the measurement noise in the sensor outputs, as the number of sampling points is large. The five-sensor method (IF5S) developed by Fung, et al. [20, 21] employs Fourier series to determine the surface profile when there exist the straightness and tilt errors as well as the zero-adjustment values. As an extension, an eight-sensor method called F8S is reported [22]. The sensor configurations of both IF5S and F8S need to be chosen suitably, and the length of the test section is determined by the size of the slider. Based on the reversal method [23] and the generalized three-sensor method, Gao et al. [24, 25] developed the reversal six-sensor method. By scanning the two opposed surface profiles of a cylinder simultaneously, the method can be used for estimating the profiles and the straightness and tilt errors, with the zero-adjustment values taken into account. Because the measurement system either contains an additional cylinder or has the reversal function, it is difficult to integrate the measurement system with the linear slideway. In addition, the previous researches have paid little attention to the influences of the measurement noise in the sensor outputs, the sensor gain error and the positioning error of the linear slideway on the multi-sensor methods.

In this paper, a new four-sensor method with an improved measurement system is proposed to separate simultaneously the straightness and tilt errors of a linear slideway, with the zero-adjustment values taken into account. The measurement system allows achieving the adjustable sensor spacing and the high lateral resolution, and avoids the sensor gain error. The proposed method has some advantages, such as suitable for the test section of any length, needless to pre-measure the zero-adjustment values and the surface profile accurately, and favorable propagations of the residuals induced by the noise and the positioning errors. This paper is organized as follows. The new method and the improved system are explained in detail in Section 2. To analyze the influences of the measurement noise in the senor outputs and the positioning errors of the sensors and the slideway on the method, a series of computer simulations are conducted in Section 3. In Section 4, an experiment is implemented to verify the feasibility of the method.

2 New Error Separation Method

The improved measurement system, as shown in Figure 1, contains a displacement sensor and a sensor stage with accurate movement along X-axis. The system is attached to a linear slideway. The relative displacement between the reference surface and the slideway is detected by the sensor. Different configurations are formed by adjusting the position of the sensor relative to the stage. The combination of these configurations constructs an improved multi-sensor measurement system that can realize the function of the traditional multi-sensor measurement system. The improved system has some advantages, such as adjustable sensor spacing and no gain error. A function $f(x)$ is introduced to describe the reference surface profile, and the straightness and tilt errors of the slideway are represented by the functions $S(x)$ and $\gamma(x)$ respectively. The sensor associated with the ith configuration is named the sensor i ($i \geq 1$). For the sensor i, the zero-adjustment value relative to the sensor 1 is defined as e_i and the spacing relative to the sensor $(i-1)$ set to $D_i = s_i \times \Delta x$. s_i is an integer and Δx (in Figure 1) denotes the lateral resolution. Obviously, both e_1 and s_1 equal 0. e_i describes the effect caused by the geometric errors of the sensor stage on the sensor output. If N denotes the total sampling number, the position of any sampling point can be described as $x_n = n \times \Delta x$, $n = 0$, 1,…, $(N-1)$. Then, the length of the measured reference surface is $L_0 = (N-1) \times \Delta x$ and the travel of the slideway $L = (N - s_2 - s_3 - s_4 - 1) \times \Delta x$. Because the sensor stage
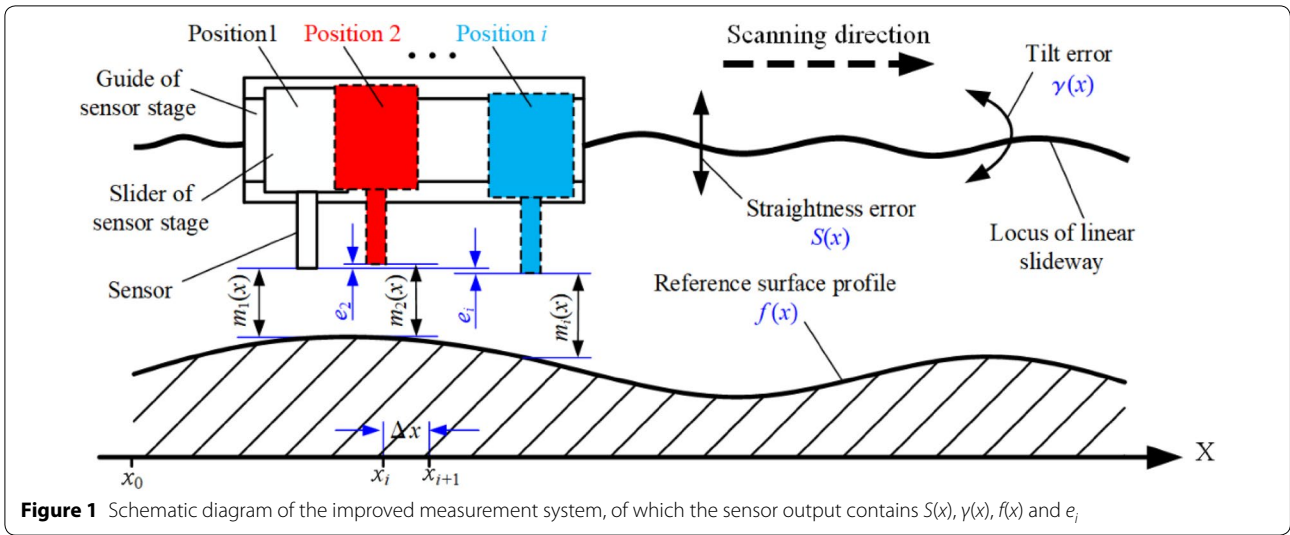
Zhao *et al. Chin. J. Mech. Eng.* (2019) 32:24

Page 3 of 11

Figure 1 Schematic diagram of the improved measurement system, of which the sensor output contains $S(x)$, $\gamma(x)$, $f(x)$ and e_i

isn't calibrated accurately beforehand, e_i $(i \neq 1)$ is unknown. Based on the above information, the output $m_i(x_n)$ of the sensor i $(i=1, 2, 3, 4)$ at the sampling point x_n can be expressed as Eq. (1), $n=0, 1, ..., N - s_2 - s_3 - s_4 - 1$. If e_i or $\gamma(x)$ is either ignored or known, the improved system is able to identify $f(x)$ from $m_i(x_n)$ according to the four-sensor methods in Refs. [18, 19]. However, in general, e_i and $\gamma(x)$ are non-ignorable and unknown, so the methods are unavailable. For this problem, a new four-sensor method is developed as follows:

$$\begin{cases} m_1(x_n) = f(x_n) + S(x_n) + e_1, \\ m_2(x_n) = f(x_n + D_2) + S(x_n) + D_2 \cdot \gamma(x_n) + e_2, \\ m_3(x_n) = f(x_n + D_2 + D_3) + S(x_n) \\ \qquad + (D_2 + D_3) \cdot \gamma(x_n) + e_3, \\ m_4(x_n) = f(x_n + D_2 + D_3 + D_4) + S(x_n) \\ \qquad + (D_2 + D_3 + D_4) \cdot \gamma(x_n) + e_4, \end{cases} \quad (e_1 = 0)$$

(1)

To eliminate the influences of $S(x_n)$ and $\gamma(x_n)$, the following equation is derived from Eq. (1):

$$C \begin{pmatrix} m_1(x_n) \\ m_2(x_n) \\ m_3(x_n) \\ m_4(x_n) \end{pmatrix} = C \begin{pmatrix} f(x_n) \\ f(x_n + D_2) \\ f(x_n + D_2 + D_3) \\ f(x_n + D_2 + D_3 + D_4) \end{pmatrix} + C \begin{pmatrix} e_1 \\ e_2 \\ e_3 \\ e_4 \end{pmatrix},$$

(2)

where

$$C = \begin{bmatrix} 1 & -\frac{D_2+D_3}{D_3} & \frac{D_2}{D_3} & 0 \\ 1 & -\frac{D_2+D_3+D_4}{D_3+D_4} & 0 & \frac{D_2}{D_3+D_4} \\ 1 & 0 & -\frac{D_2+D_3+D_4}{D_4} & \frac{D_2+D_3}{D_4} \\ 0 & 1 & -\frac{D_3+D_4}{D_4} & \frac{D_3}{D_4} \end{bmatrix}.$$

(3)

A system of linear equations is then built according to Eq. (2):

$$A_0 X = b_0.$$

(4)

A_0, b_0 and X are given in Eqs. (5)–(7):

$$A_0 = \begin{bmatrix} c_1 \\ \vdots \\ c_i \\ \vdots \\ c_p \end{bmatrix}, \quad (p = N - s_2 - s_3 - s_4 - 1),$$

(5)

$$b_0 = \begin{bmatrix} g_1(x_0) & \cdots & g_4(x_0) & \cdots & g_1(x_p) & \cdots & g_4(x_p) \end{bmatrix}^T,$$

(6)

$$X = \begin{bmatrix} f(x_0) & \cdots & f(x_{N-1}) & \Delta e_1 & \cdots & \Delta e_4 \end{bmatrix}^T,$$

(7)

where

$$c_i = \begin{bmatrix} 0_{4 \times (i-1)} & C & 0_{4 \times (N-i-3)} & I_{4 \times 4} \end{bmatrix},$$

(8)

$$\begin{bmatrix} g_1(x_n) \\ g_2(x_n) \\ g_3(x_n) \\ g_4(x_n) \end{bmatrix} = C \begin{bmatrix} m_1(x_n) \\ m_2(x_n) \\ m_3(x_n) \\ m_4(x_n) \end{bmatrix}, \quad n \in [1, p],$$

(9)

$$\begin{bmatrix} \Delta e_1 \\ \Delta e_2 \\ \Delta e_3 \\ \Delta e_4 \end{bmatrix} = C \begin{bmatrix} e_1 \\ e_2 \\ e_3 \\ e_4 \end{bmatrix}.$$

(10)

However, the rank of A_0 is deficient, indicating that there are innumerable solutions for the linear system [26]. In other words, $f(x_n)$ cannot be estimated

Zhao *et al. Chin. J. Mech. Eng.* (2019) 32:24

Page 4 of 11

uniquely. Therefore, it is necessary to incorporate additional information to obtain a definite solution.

To restrict the reconstruction of the reference surface profile, a straight line is defined by applying Eq. (11). The shape of $f(x)$ relative to the straight line is then determined uniquely.

$$\begin{cases} f(x_0) = 0, \\ f(x_{N-1}) = 0. \end{cases} \tag{11}$$

When $s_2 = s_3 = 1$, Eq. (12) is derived by using the outputs of the sensors 1, 2 and 3 based on the generalized three-sensor method [11, 13]. Then, Δe_1 can be calculated.

$$f(x_{N-1}) = \sum_{i=1}^{N-1} (N-i)g_1(x_{i-1}) - \frac{N(N-1)}{2}\Delta e_1. \tag{12}$$

From Eq. (10), the relationships described in Eq. (13) are deduced:

$$\begin{cases} \Delta e_3 + \frac{s_3(s_2+s_3+s_4)}{s_2 s_4}\Delta e_1 - \frac{(s_2+s_3)(s_3+s_4)}{s_2 s_4}\Delta e_2 = 0, \\ \Delta e_4 + \frac{s_3(s_3+s_4)}{s_2 s_4}\Delta e_1 - \frac{s_3(s_3+s_4)}{s_2 s_4}\Delta e_2 = 0. \end{cases} \tag{13}$$

The constraints given in Eqs. (11)–(13) and the original linear system in Eq. (4) are then written compactly to construct a new system of linear equations as follows:

$$AX = b, \tag{14}$$

where A and b are given in Eqs. (15), (16). The column vector b is constructed by all the sensor outputs. The coefficient matrix A that owns the full rank is formed by D_i. The column vector X involves $f(x_n)$, $n = 0, 1, ..., (N-1)$, and Δe_i, $i = 1, 2, 3, 4$. The common technique to solve the linear system is the least squares method [27]. The condition number of the matrix A determines the quality of the least squares solution. However, A appears ill-conditioned. Figure 2 illustrates the variation of the condition number of A with the number of sampling points N, when $D_2 = D_3 = 5$ mm, $D_4 = 25$ mm and $\Delta x = 5$ mm. As N equals 30 and 200, the condition number is about 6×10^3 and 2.4×10^6, respectively. The increase in the condition number of A makes the least squares solution more sensitive to the perturbation in b [28]. In other words, $\bar{f}(x_n)$ may fluctuate drastically with the measurement noise in $m_i(x_n)$.

$$A = \begin{bmatrix} \multicolumn{6}{c}{A_0} \\ 1 & \cdots & 0 & 0 & 0 & 0 & 0 \\ 0 & \cdots & 1 & 0 & 0 & 0 & 0 \\ 0 & \cdots & 0 & 1 & 0 & 0 & 0 \\ 0 & \cdots & 0 & \frac{s_3(s_2+s_3+s_4)}{s_2 s_4} & -\frac{(s_2+s_3)(s_3+s_4)}{s_2 s_4} & 1 & 0 \\ 0 & \cdots & 0 & \frac{s_3(s_3+s_4)}{s_2 s_4} & -\frac{s_3(s_3+s_4)}{s_2 s_4} & 0 & 1 \end{bmatrix}, \tag{15}$$

Figure 2 Variation of the condition number of the coefficient matrix A with the number of sampling points N

$$b = \begin{bmatrix} b_0^{\mathrm{T}} & 0 & 0 & \frac{2}{N(N-1)}\sum_{i=1}^{N-1}(N-i)g_1(x_{i-1}) & 0 & 0 \end{bmatrix}^{\mathrm{T}}. \tag{16}$$

To single out a useful and stable solution, the Tikhonov regularization method [29, 30] is utilized. The regularized solution X_λ is defined as the minimizer of the following weighted combination of the residual $\|AX - b\|^2$ and the side constraint $\|X\|^2$, as shown in Eq. (17):

$$X_\lambda = \min\left\{\|AX - b\|^2 + \lambda^2\|X\|^2\right\} = \left(A^{\mathrm{T}}A + \lambda^2 I\right)^{-1}A^{\mathrm{T}}b, \tag{17}$$

where I is the unit matrix and λ denotes the regularization parameter. As described in Eq. (17), λ controls the weight between the side constraint and the residual as well as the sensitivity of X_λ to the perturbations in A and b. Therefore, it should be selected carefully. The L-curve criterion [29, 30] described by $\left(\log\|AX_\lambda - b\|, \log\|X_\lambda\|\right)$ is used to calculate the optimal parameter λ_p. After λ_p is determined, the estimate of $f(x_n)$ can be solved from the system of linear equations in Eq. (14), which is marked as $\bar{f}(x_n)$. $S(x_n)$ and $\gamma(x_n)$ are then separated directly based on Eq. (1), as shown in Eqs. (18), and (19).

$$S(x_n) = m_1(x_n) - \bar{f}(x_n), \tag{18}$$

$$\gamma(x_n) = \frac{1}{D_2 + D_3 + D_4}\left\{m_4(x_n) - m_1(x_n) \right. \\ \left. - \left[\bar{f}(x_n + D_2 + D_3 + D_4) - \bar{f}(x_n)\right] - e_4\right\}. \tag{19}$$

Due to the term $e_4/(D_2 + D_3 + D_4)$ being constant, it has no influence on the shape of $\gamma(x)$. So far, the new four-sensor method for identifying the straightness and tilt errors has been developed.

Zhao *et al. Chin. J. Mech. Eng.* (2019) 32:24
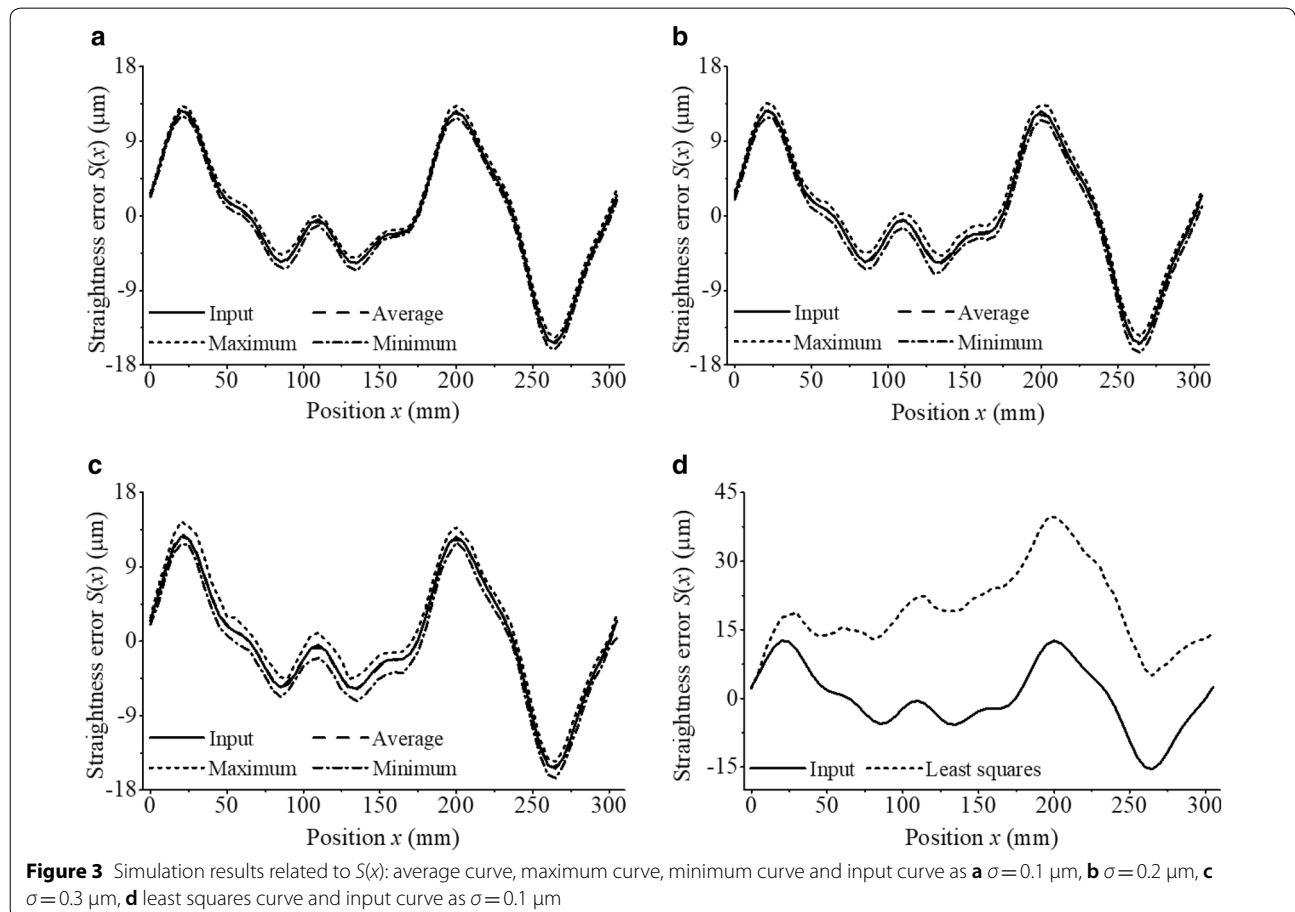
Page 5 of 11
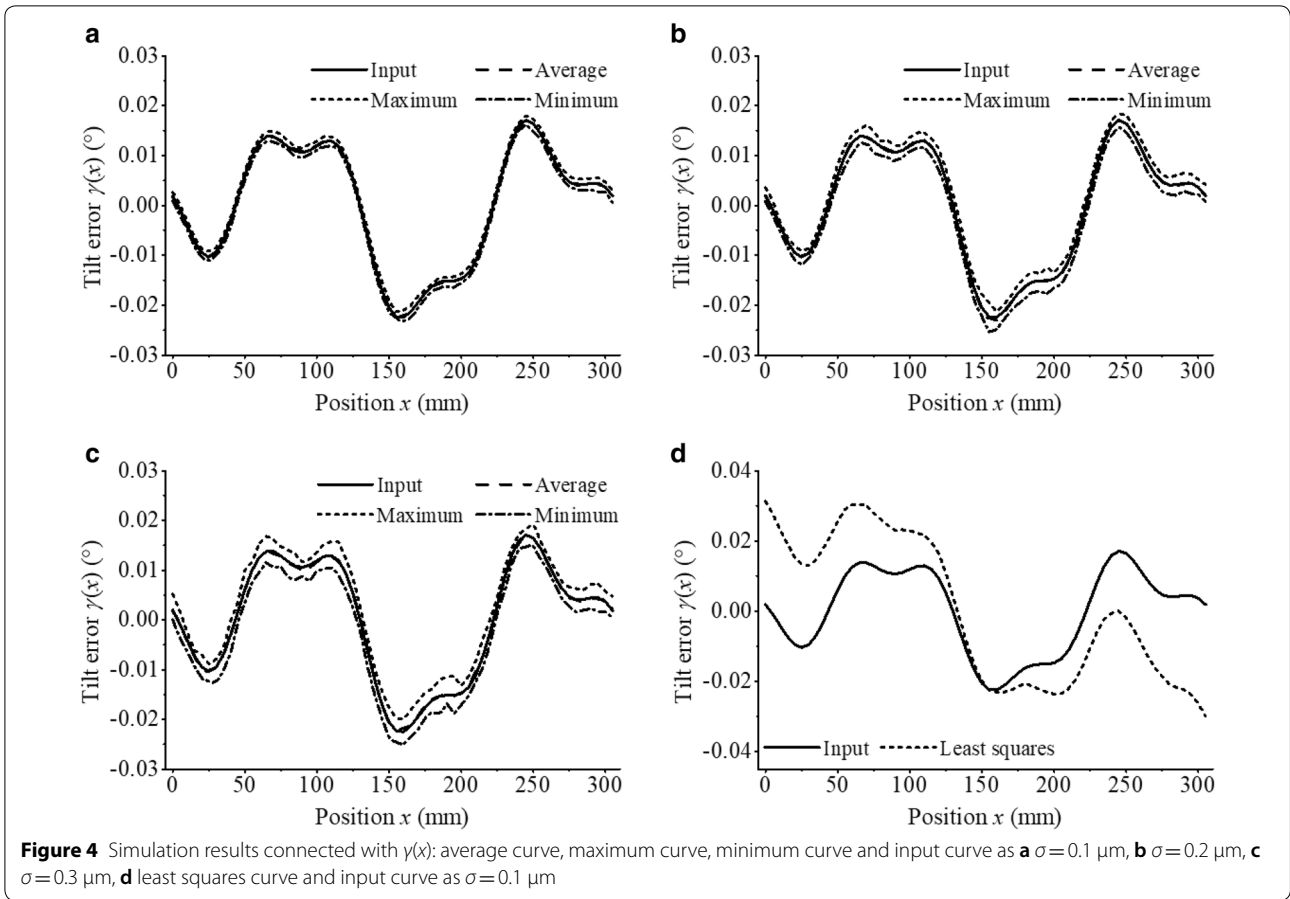
3 Simulation Verifications

A simulation platform is constructed by using MAT-LAB to evaluate the proposed method. To represent the measurement noise, a Gaussian distribution with the zero mean and the standard deviation σ is added in $m_i(x_n)$. $S(x)$ and $\gamma(x)$ are predefined as the input values to compare with the simulation results. σ is assigned with three values, namely 0.1 μm, 0.2 μm and 0.3 μm, to analyze the influence of the noise on the simulation results. Other parameters are set as $\Delta x = 5$ mm, $s_4 = 5$, $N = 69$. So, $L_0 = 340$ mm, $L = 305$ mm, $D_2 = D_3 = 5$ mm, and $D_4 = 25$ mm. During the measuring process, the sensor of the improved system needs to be adjusted to different positions. Therefore, it is necessary to investigate the effect of the positioning error $PE1$ of the sensor on $S(x)$ and $\gamma(x)$. $PE1$ is introduced by changing the values of D_2, D_3 and D_4 to 5.012mm, 4.985mm and 25.02 mm, respectively. An analysis is also conducted on the influence caused by the positioning error $PE2$ (unit: μm) of the linear slideway expressed by Eq. (20). In this section, two examples are discussed.

$$PE2 = -10\sin\left(\frac{2\pi}{L}x + \frac{1}{12}\pi\right) - 3\sin\left(\frac{6\pi}{L}x + \frac{1}{2}\pi\right) + 4.5\sin\left(\frac{2\pi}{L}x + \frac{5}{6}\pi\right).$$

(20)

Example 1 $S(x)$ (unit: μm) and $\gamma(x)$ (unit: degree) are described by Eqs. (21), (22), of which the curves are given with the solid line in Figures 3 and 4. In addition, $f(x)$ (unit: μm) is defined as Eq. (23).

When the sensor outputs are free of the noise and the positioning errors, the simulation results for $S(x)$ and $\gamma(x)$ are almost same as the input values. As $\sigma = 0.1$ μm, 0.2 μm and 0.3 μm, the platform is executed 20 times for each value without the positioning errors. The consequences associated with $S(x)$ are shown in Figure 3(a)–(c), which plot the average, maximum and minimum of the simulation results at each sampling point. It can be seen that the average curve is in accordance with the input curve except a small difference, and that the maximum

Figure 3 Simulation results related to $S(x)$: average curve, maximum curve, minimum curve and input curve as **a** $\sigma = 0.1$ μm, **b** $\sigma = 0.2$ μm, **c** $\sigma = 0.3$ μm, **d** least squares curve and input curve as $\sigma = 0.1$ μm

Figure 4 Simulation results connected with γ(x): average curve, maximum curve, minimum curve and input curve as **a** σ = 0.1 μm, **b** σ = 0.2 μm, **c** σ = 0.3 μm, **d** least squares curve and input curve as σ = 0.1 μm

and minimum curves have the similar shape to the input curve. The curve in Figure 3(d) is obtained, as Eq. (14) is solved by using the least squares method under the condition of σ = 0.1 μm. There is a significant deviation, indicating that the least squares method is unsuitable to solve the linear system with the ill-conditioned coefficient matrix. The similar conclusions can be drawn for γ(x) from the simulation results in Figure 4.

$$S(x) = 8.075 \sin\left(\frac{4\pi}{L}x\right) + 5.7 \sin\left(\frac{6\pi}{L}x + \frac{5}{18}\pi\right)$$
$$- 1.9 \sin\left(\frac{14\pi}{L}x + \frac{1}{2}\pi\right),$$

(21)

$$\gamma(x) = 0.008 \sin\left(\frac{2\pi}{L}x + \frac{1}{3}\pi\right) - 0.014 \sin\left(\frac{4\pi}{L}x + \frac{1}{4}\pi\right)$$
$$+ 0.005 \sin\left(\frac{10\pi}{L}x + \frac{7}{12}\pi\right),$$

(22)

$$f(x) = 5 \sin\left(\frac{10\pi}{L_0}x\right).$$

(23)

To represent the discrepancies in Figure 3(a)–(c) and Figure 4(a)–(c), two types of parameters are introduced: $\Delta S_{\max}/\Delta\gamma_{\max}$ signifying the maximum of the residuals of the simulation results relative to the input curve, and $\Delta S^a_{\max}/\Delta\gamma^a_{\max}$ denoting the maximum residual between the average curve and the input curve. For the three cases, $\Delta S_{\max}$ is less than 1.1 μm, 1.6 μm and 2.3 μm, while $\Delta S^a_{\max}$ is less than 0.15 μm, 0.26 μm and 0.3 μm. $\Delta\gamma_{\max}$ is 1.8×10^{-3} degree, 3.2×10^{-3} degree and 3.9×10^{-3} degree, while $\Delta\gamma^a_{\max}$ is 2.5×10^{-4} degree, 6.5×10^{-4} degree and 7.2×10^{-4} degree. In summary, Figures 3 and 4 indicate that the proposed method can separate $S(x)$ and $\gamma(x)$ from the sensor outputs with good accuracy. Moreover, $\Delta S_{\max}$, $\Delta S^a_{\max}$, $\Delta\gamma_{\max}$ and $\Delta\gamma^a_{\max}$ are proportional to the standard deviation σ.

When only *PE*1 exists and σ = 0 μm, the residuals of the simulation results of $S(x)$ and $\gamma(x)$ relative to their input values are displayed as the solid lines in Figure 5. The maximum residual for $S(x)$ is 0.1 μm, while that for $\gamma(x)$ is less than 1.0×10^{-4} degree. From the dashed lines in Figure 5, the maximum residuals caused by *PE*2 for $S(x)$ and $\gamma(x)$ are 0.15 μm and 1.0×10^{-4} degree, respectively. Figure 5 reveals that the positioning errors

Zhao *et al. Chin. J. Mech. Eng.*   (2019) 32:24

Page 7 of 11

Figure 5 Residuals caused by the positioning errors *PE*1 and *PE*2 as $\sigma = 0$ μm
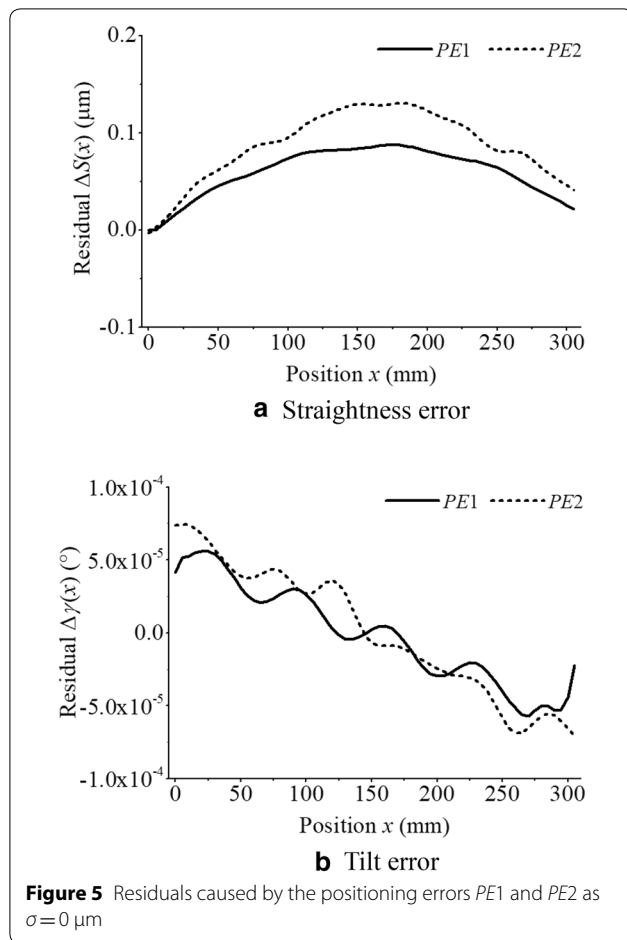
have slight influences on the estimates of $S(x)$ and $\gamma(x)$ obtained by the proposed method.

Example 2 When $f(x)$ is set to Eq. (24), the variations of the residuals between the simulation results and the input values with the harmonic order k are investigated as $\sigma = 0.2$ μm.

$$f(x) = 5\sin\left(k\frac{2\pi}{L_0}x\right) + 5\sin\left(\frac{20\pi}{L_0}x\right). \quad (24)$$

In the simulation, $S(x)$ and $\gamma(x)$ are represented by Eqs. (21), (22). For each k, the maximum and the average of the residuals between the simulation results and the input value for $S(x)$ at each sampling point are collected (described in Figure 6(a)), after the platform is performed 20 times. It can be seen that ΔS_{max} and ΔS_{max}^a are less than 2.6 μm and 0.6 μm. The results related to $\gamma(x)$ are given in Figure 6(b), showing that $\Delta\gamma_{max}$ and $\Delta\gamma_{max}^a$ are about 5×10^{-3} degree and 9×10^{-4} degree, respectively. The relationships of the residuals induced by *PE*1 and

*PE*2 relative to k are also analyzed in the case of $\sigma = 0$ μm, as shown in Figure 7. The maximum residuals for $S(x)$ are both less than 0.4 μm, while those for $\gamma(x)$ are smaller than 3×10^{-4} degree, implying that the positioning errors have very tiny influences on $S(x)$ and $\gamma(x)$.

In short, the proposed method can guarantee favorable propagations of the residuals induced by the noise and the positioning errors as the harmonic order k varies.

4 Experimental Results and Discussion

An experiment is designed for further verification. As shown in Figure 8, a displacement sensor is developed, comprising the probe, the flexure-based amplifier, the flexure-based loader and the encoder. The input displacement of the probe is amplified by the amplifier and then detected by the encoder. The sensor has a measurement range of 0.2 mm with the resolution of 0.035 μm. The input stiffness of the sensor is about 0.3 N/μm, so the probe wear isn't considered. The displacement sensor and a micro-platform form the measurement system which is fixed on the slider of the linear slideway. The sensor position can be adjusted manually by the micrometer. A pre-displacement is applied to the probe by the loader, to press firmly the probe against the side of the linear slideway during the measuring process.

The coordinate system *OXY* is established, and its *X*-axis satisfies the constraint described in Eq. (11). The angles of the probe relative to the guide of the micro-platform and the reference surface are both limited in 90 ± 0.1 degree. The sensor output is collected by a clipper card and recorded by an industrial computer. The configuration parameters for the measurement system are as follows: $\Delta x = 5$ mm, $D_2 = D_3 = 5$ mm, $D_4 = 25$ mm, $N = 69$. The environment temperature is controlled at 20 ± 0.5 °C.

The experiment is repeated six times. Then, the sensor outputs are averaged and filtered to reduce the measurement noise. Based on the new four-sensor method, the straightness and tilt errors are calculated and described (in *OXY*) as $S_a(x)$ and $\gamma_a(x)$ in Figure 9. In addition, the obtained surface profile is shown in Figure 10. The straightness and tilt errors are also measured four times by a laser interferometer with the linear accuracy of ± 0.5 μm and the angular accuracy of ± 1 arcsec. The related results (in the coordinate system $O_mX_mY_m$ of the laser interferometer) are plotted in Figure 9, named $S_l(x)$ and $\gamma_l(x)$. It is improper to compare $S_a(x)$ with $S_l(x)$ directly, because of the different coordinate systems. Taking the $O_mX_mY_m$ as the reference, the *OXY* is rotated so that the 2-norm of $S_l^m(x) - S_a(x)$ is minimum. Where $S_l^m(x)$ is the average of the four values of $S_l(x)$. This situation indicates that the *OXY* is the same as the $O_mX_mY_m$.
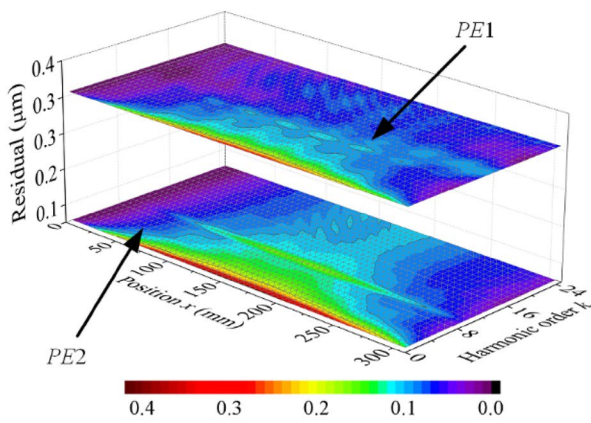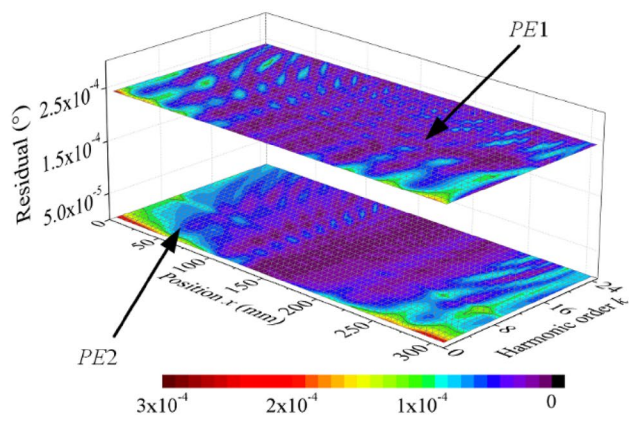
Zhao *et al. Chin. J. Mech. Eng.*   (2019) 32:24

Page 8 of 11
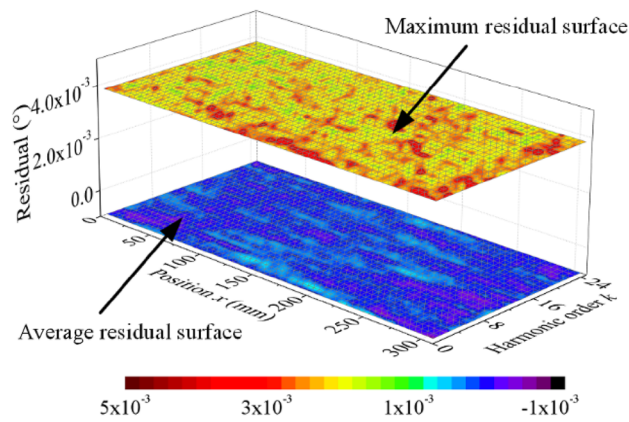
Figure 6 Variations of the average and maximum of the residuals caused by the noise ($\sigma = 0.2$ μm) at the sampling points with the harmonic order k

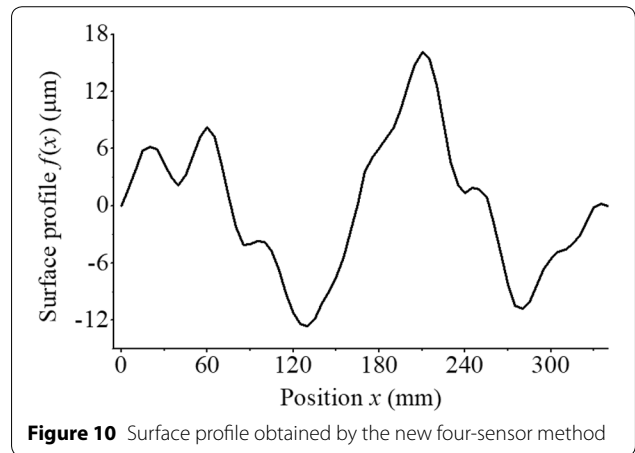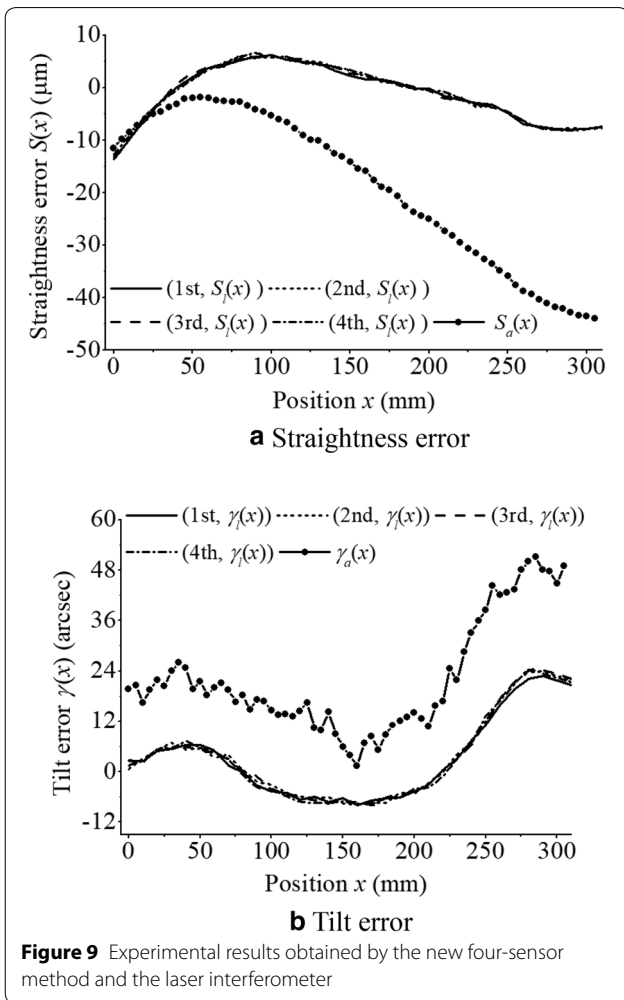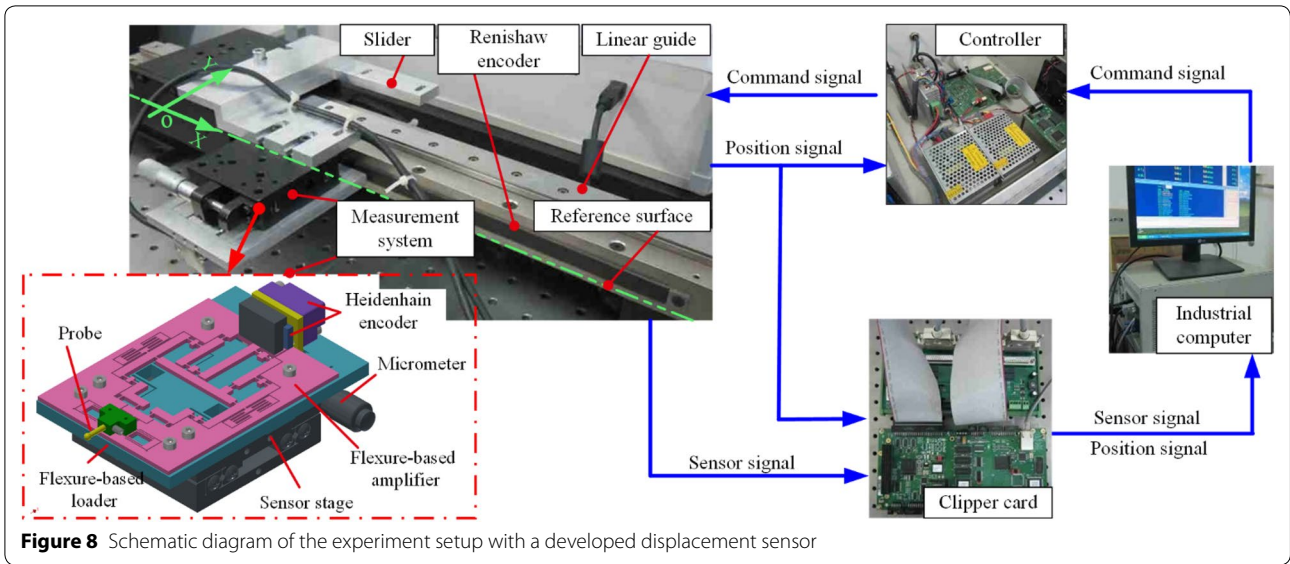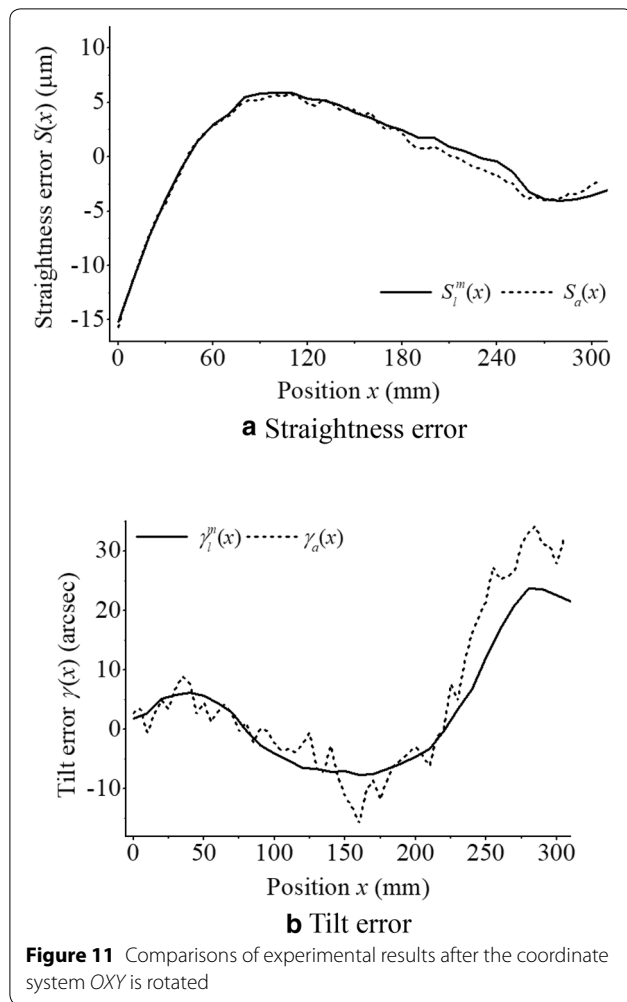**Figure 7** Relationships between the residuals caused by the positioning errors *PE*1 and *PE*2 at the sampling points and the harmonic order k

Figure 8 Schematic diagram of the experiment setup with a developed displacement sensor

a Straightness error

b Tilt error

Figure 9 Experimental results obtained by the new four-sensor method and the laser interferometer

Figure 10 Surface profile obtained by the new four-sensor method

After the rotation, $S_a(x)$ given in Figure 11(a) is consistent with $S_l^m(x)$ and the maximum deviation between them is less than 2.5 μm. The similar operation is performed on $\gamma_a(x)$ and $\gamma_l(x)$. As shown in Figure 11(b), the final results have the similar trend and the maximum deviation is about 11 arcsec. Therefore, the proposed four-sensor method together with the improved measurement system is able to identify the straightness and tilt errors of the linear slideway. The discrepancies in Figure 11 might be mainly caused by the measurement noise in $m_i(x_n)$ from the repeatability of the straightness and tilt errors, the interferometer accuracy and the sensor accuracy. Moreover, the positioning errors of the sensor stage and the slideway may also produce a difference.

Zhao *et al. Chin. J. Mech. Eng.*   (2019) 32:24

Page 10 of 11

Figure 11 Comparisons of experimental results after the coordinate system *OXY* is rotated

5 Conclusions

With the adoption of an improved measurement system, a new four-sensor method is presented to identify the straightness and tilt errors of a linear slideway from the sensor outputs. The reference surface profile could be obtained simultaneously. Its feasibility is evaluated by computer simulations and experiment. From the results, some conclusions are summarized as follows.

(1) The measurement system allows achieving the adjustable sensor spacing and the high lateral resolution, and avoids the sensor gain error. The proposed method has some advantages, such as suitable for the test section of any length as well as needless to pre-measure the zero-adjustment values and the reference surface profile accurately.

(2) The method is feasible and can guarantee the favorable propagation of the residual caused by the measurement noise in the sensor outputs. In addition, it is influenced slightly by the positioning errors of the sensor and the slideway.

(3) The maximum discrepancy between the experimental results associated with the straightness error is less than 2.5 µm. The results corresponding to the tilt error have the similar trend.

Authors' Contributions
KC and HD was in charge of the conceptualization; Lei Zhao proposed and analyzed the methodology; Lei Zhao and Liang Zhao built the experiment setup and conducted the experiment; Lei Zhao wrote the original draft. All authors read and approved the final manuscript.

Author Details
[1] School of Mechatronics Engineering, Harbin Institute of Technology, Harbin 150001, China. [2] College of Engineering, Design and Physical Sciences, Brunel University, London, Uxbridge UB 3PH, UK.

Authors' Information
Lei Zhao, born in 1987, is currently a doctoral candidate at *School of Mechatronics Engineering, Harbin Institute of Technology, China*. He received his mater degree from *Harbin Institute of Technology, China*, in 2012. His research interests include precision metrology and precision design.

   Kai Cheng, born in 1961, is currently a Chair Professor at *College of Engineering, Design and Physical Sciences, Brunel University London, United Kingdom*. He received his PhD in 1994 from *Liverpool John Moores University, United Kingdom*. His current research interests include precision and micro manufacturing, design of high precision machine tools, sustainable manufacturing systems and e-manufacturing.

   Hui Ding, born in 1981, is currently an associate professor at *School of Mechatronics Engineering, Harbin Institute of Technology in China*. He received his PhD from *Harbin Institute of Technology*, *China*, in 2011. His current research interests focus on precision and micro manufacturing, smart cutting tool, and micro-featured engineering surfaces.

   Liang Zhao, born in 1987, is currently an engineer and also a doctoral candidate at *School of Mechatronics Engineering, Harbin Institute of Technology, China*. His research interests include ultraprecision machining and micro manufacturing.

References
[1]   S J Zhang, S To, S J Wang, et al. A review of surface roughness generation in ultra-precision machining. *International Journal of Machine Tools and Manufacture*, 2015, 1(91): 76–95.
[2]   Chinese Mechanical Engineering Society. *Technology roadmaps of Chinese mechanical engineering*. 2nd ed. Beijing: Popular Science Press, 2016. (in Chinese)
[3]   P Yang, T Takamura, S Takahashi, et al. Development of high-precision micro-coordinate measuring machine: multi-probe measurement system for measuring yaw and straightness motion error of XY linear stage. *Precision Engineering*, 2011, 35(3): 424–430.
[4]   K C Fan, F Cheng, H Y Wang, et al. The system and the mechatronics of a pagoda type micro-CMM. *International Journal of Nanomanufacturing*, 2012, 8: 67–86.

Zhao *et al. Chin. J. Mech. Eng.* (2019) 32:24

Page 11 of 11

[5] Q Huang, G B Zhang. Precision design for machine tool based on error prediction. *Chinese Journal of Mechanical Engineering*, 2013, 26(1): 151–157.

[6] H Schwenke, W Knapp, H Haitjema, et al. Geometric error measurement and compensation of machines - an update. *CIRP Annals - Manufacturing Technology*, 2008, 57(2): 660–675.

[7] The International Organization for Standardization. ISO 230-1–2012 Test code for machine tools – Part 1: geometric accuracy of machines operating under no-load or quasi-static conditions. Geneva: ISO Office, 2012.

[8] J Li, F G Xie, B Mei, et al. Analysis on the research status of volumetric positioning accuracy improvement methods for five-axis NC machine tools. *Journal of Mechanical Engineering*, 2017, 53(7): 113–128. (in Chinese)

[9] S W Zhu, G F Ding, S F Qin, et al. Integrated geometric error modeling, identification and compensation of CNC machine tools. *International Journal of Machine Tools and Manufacture*, 2012, 52(1): 24–29.

[10] D D Zhai, S Y Chen, Z Q Yin, et al. Review of self-referenced measurement algorithms: bridging lateral shearing interferometry and multi-probe error separation. *Frontiers of Mechanical Engineering*, 2017, 12: 143–157.

[11] Z Q Yin. *Research on ultra-precision measuring straightness and surface microtopography analysis*. Changsha: National University of Defense Technology, 2003. (in Chinese)

[12] W Gao, S Kiyono. High accuracy profile measurement of a machined surface by the combined method. *Measurement*, 1996, 19(1): 55–64.

[13] Z Liu, S Jiang, X Li, et al. Precision measurement of X-axis stage mirror profile in scanning beam interference lithography by three-probe system based on bidirectional integration model. *Optics Express*, 2017, 25(9): 10312–10321.

[14] W Gao, S Kiyono. On-machine profile measurement of machined surface using the combined three-point method. *JSME International Journal Series C: Mechanical Systems, Machine Elements and Manufacturing*, 1997, 40(2): 253–259.

[15] Z Q Yin, S Y Li. High accuracy error separation technique for on-machine measuring straightness. *Precision Engineering*, 2006, 30(2): 192–200.

[16] Z Q Yin, S Y Li, F J Tian. Exact reconstruction method for on-machine measurement of profile. *Precision Engineering*, 2014, 38(4): 969–978.

[17] I Fujimoto, K Nishimura, T Takatsuji, et al. A technique to measure the flatness of next-generation 450 mm wafers using a three-point method with an autonomous calibration function. *Precision Engineering*, 2012, 36(2): 270–280.

[18] I Weingartner, C Elster. System of four distance sensors for high-accuracy measurement of topography. *Precision Engineering*, 2004, 28(2): 164–170.

[19] A Wiegmann, C Elster, R D Geckeler, et al. Stability analysis for the TMS method: influence of high spatial frequencies. *Optical Measurement Systems for Industrial Inspection V*, Munich, Germany, June 17–21, 2007: 661618-1–661618-9.

[20] E H K Fung, M Zhu. An improved Fourier five-sensor (IF5S) method for separating straightness and yawing errors of a linear slide based on multiple sensor parameter sets and least square regression technique. *Measurement*, 2012, 45(5): 1323–1330.

[21] E H K Fung. An experimental five-sensor system for measuring straightness and yawing motion errors of a linear slide. *Measurement Science and Technology*, 2008, 19(7): 075102.

[22] E H K Fung, M Zhu, X Z Zhang, et al. A novel Fourier-Eight-Sensor (F8S) method for separating straightness, yawing and rolling motion errors of a linear slide. *Measurement*, 2014, 47: 777–788.

[23] C J Evans, R J Hocken, W T Estler, et al. Self-calibration: reversal, redundancy, error separation, and 'absolute testing'. *CIRP Annals*, 1996, 45(2): 617–634.

[24] W Gao, J Yokoyama, H Kojima, et al. Precision measurement of cylinder straightness using a scanning multi-probe system. *Precision Engineering*, 2002, 26(3): 279–288.

[25] W Gao. *Precision nanometrology: sensors and measuring systems for nanomanufacturing*. London: Springer, 2010.

[26] D C Lay, S R Lay, J J McDonald. *Linear algebra and its applications*. 5th ed. New York: Pearson, 2015.

[27] A Uncini. *Fundamentals of adaptive signal processing*. Cham: Springer International Publishing, 2015.

[28] V K Ivanov, V V Vasin, V P Tanana. *Theory of linear ill-posed problems and its applications*. Walter de Gruyter, 2013.

[29] M Fuhry, L Reichel. A new Tikhonov regularization method. *Numerical Algorithms*, 2012, 59(3): 433–445.

[30] K Ito, B Jin. *Inverse problems: Tikhonov theory and algorithms*. Singapore: World Scientific, 2014.